

Cite this: *CrystEngComm*, 2012, 14, 8562–8568

www.rsc.org/crystengcomm

PAPER

Spontaneous water release inducing nucleation during the nonaqueous synthesis of TiO₂ nanoparticles†

Mandy Zimmermann and Georg Garnweitner*

Received 11th June 2012, Accepted 9th October 2012

DOI: 10.1039/c2ce25934f

The formation of anatase nanoparticles by reaction of titanium(IV) isopropoxide in benzyl alcohol was studied. In contrast to previous reports on the nonaqueous synthesis, in this system the particle formation occurs within a very limited time span in the course of the synthesis, concurrently to a fast step-type pressure increase within the closed reaction system. By Karl Fischer titration and ¹H NMR spectroscopy of both the liquid and the gaseous phase at different stages of the reaction, it is shown that water formation occurs during the pressure increase due to catalytic ether formation from benzyl alcohol. The generated water leads to instant nucleation and fast growth of crystalline nanoparticles, which is traced by powder X-ray diffraction as well as small-angle X-ray scattering and thereby shown to play a crucial role in the particle formation process.

Introduction

Highly crystalline metal oxide nanoparticles of defined size are in great demand for a variety of applications. Titanium dioxide nanoparticles in particular have been of high interest due to their excellent photocatalytic properties^{1–4} but also their antibacterial performance⁵ and potential use in dye-sensitized solar cells^{6–9} as well as for cancer treatment.^{10,11} For their synthesis, there are different techniques available, from gas phase methods producing metal oxide nanoparticles in large quantities at relatively low cost^{12,13} to liquid-based methods that generally are more controllable as well as flexible with regard to the particle characteristics.¹⁴ In the conventional aqueous sol–gel synthesis, however, metal oxides are mostly obtained in high crystallinity only after an additional calcination step. In the last decade, various nonaqueous techniques were established, such as the benzyl alcohol route being broadly applicable not only for TiO₂ but for a multitude of metal oxides and leading directly to highly crystalline nanoparticles.^{15–18} This route includes the reaction of a molecular precursor, such as a metal alkoxide, with the organic solvent benzyl alcohol under relatively mild conditions, resulting in well-defined nanoparticles.

However, the detailed reaction mechanisms and the formation mechanism of the resulting nanoparticles are not yet fully understood for the nonaqueous synthesis. We have reported that the molecular reaction mechanisms preceding the metal oxide formation are surprisingly complex for a number of systems,¹⁹ preventing the application of simple nucleation and growth models. For the apparently similar synthesis of iron oxide

nanoparticles *via* thermal decomposition of iron oleate in an inert organic solvent, Kwon *et al.* have presented significant insights into the particle formation kinetics.^{20,21} For that system, it was shown that the decomposition of the precursor results in the formation of monomers that lead to a sudden nucleation of nanoparticles (nucleation burst), which could be described by the well-known LaMer model^{22,23} and is analogous to models of semiconductor nanocrystal nucleation and growth.^{24,25} In contrast to this method, the benzyl alcohol route is carried out at substantially lower temperatures, but also requires significantly longer reaction times of several hours to days. The molecular reaction mechanisms have been studied for the formation of TiO₂ nanoparticles *via* alkyl halide elimination, revealing the steady formation of organic side products *via* first-order kinetics.²⁶ Therefore, the formation of nanoparticles in a nucleation burst event appears unlikely, as the generated supersaturation would not be as high as for thermal decomposition processes. Similarly, a pseudo-first order kinetics was observed for the formation of ZnO *via* ester elimination.^{27,28} For the microwave-assisted synthesis of ZnO nanoparticles, it was shown that the crystal growth can be described by means of the Lifshitz–Slyozov–Wagner (LSW) theory, which points to a diffusion limited growth behavior.²⁹ It remains unclear however as to why the thermally induced nonaqueous synthesis of metal oxide nanoparticles in contrast to the microwave-assisted synthesis for many systems requires days to obtain crystalline nanoparticles despite reaction temperatures of 175–250 °C. We performed a study on the formation of iron oxide nanoparticles to elucidate this issue, and showed that the particle crystallization can be separated from nucleation, with crystallization kinetics even being dependent on the nature of the utilized reaction medium.³⁰ The nonaqueous synthesis of metal oxides hence has turned out to be a highly complex process, with the

Institute for Particle Technology, Technische Universität Braunschweig, Germany. E-mail: g.garnweitner@tu-braunschweig.de; Fax: +49 (0)531-3919633; Tel: +49 (0)531-3919615

† Electronic supplementary information (ESI) available: GC measurement, LSW plot. See DOI: 10.1039/c2ce25934f

Ligand exchange:**Ether elimination:**

BnOH: benzyl alcohol
iPrOH: isopropyl alcohol
 R: Bn/*iPr*

Scheme 1 Reaction mechanism according to the ether elimination mechanism.

precise mechanisms involved in particle nucleation still being largely unknown.

In order to shed further light on these aspects, we present investigations on the formation of TiO_2 nanoparticles by reaction of titanium isopropoxide in benzyl alcohol as a rather simple model system. The reaction of metal alkoxides was reported by us earlier to proceed in two steps *via* an ether elimination mechanism.^{31,32} The first step is a partial exchange of the isopropoxide ligand against benzyl alcohol. Subsequently, the formation of Ti–O–Ti bonds happens *via* the elimination of organic ethers analogous to the mechanism presented in Scheme 1.^{31,33} For the detailed investigation of the synthesis, we used a 1.5 L reactor system enabling the monitoring of the process temperature and pressure and moreover the withdrawal of samples at any point during the course of the synthesis.

Experimental

Synthesis of TiO_2 nanoparticles

Titanium(IV) isopropoxide (TIP, 97%) and benzyl alcohol (BnOH, 99%) (both obtained from Sigma Aldrich) were mixed in a molar ratio of 1 : 50 and transferred into a stainless steel double walled reactor of 1.5 L capacity (Polyclave type 3/1, Büchi Glas Uster) which was heated *via* an external thermostat (Huber Tango HT) at 175 °C for 48 h. The reactor was equipped with a blade agitator operated at 250 rpm, a temperature probe and a manometer enabling the recording of the temperature and the development of the pressure of the system during the whole reaction. Additionally a sampling system was installed, allowing the withdrawal of samples at different reaction times. The reaction was quenched by fast cooling of the samples in a water bath. To isolate the formed nanoparticles, the reaction suspension was centrifuged at 6500g for 10 min, washed twice with ethanol followed by centrifuging again and dried under reduced pressure at room temperature for at least 24 h. The fraction of particles that could not be separated by centrifugation was precipitated by addition of 1 mL reaction mixture to 5 mL methanol and then centrifuged, washed and dried as described above.

Characterization

The crystallite size was determined by powder X-ray diffraction (PXRD) from the dried samples with $\text{Cu K}\alpha$ radiation (Empyrean Cu LEF HR goniometer) on a Si sample holder in a range of 2θ from 20 to 90° and a step size of 0.05° (Empyrean

series 2, PANalytical, PIXcel-3D detector). For thermo-gravimetric analysis (TGA), 15–20 mg of the dried powder was analyzed with a Mettler Toledo TGA/SDTA851 instrument by heating up to 600 °C with a heating rate of 20 °C min^{-1} under oxygen atmosphere. The reaction mixture was analyzed by ^1H NMR (400 MHz, CDCl_3 or DMSO, TMS, Bruker DRX-400) and GC/MS (dichloromethane (HPLC grade), JEOL AccuTOF GC/MS, Agilent 7820A GC). Furthermore, the content of water in the reaction mixture was determined by Karl Fischer titration (Aqua 40.00, Analytik Jena). Transmission electron microscopy (TEM) images were received from a JEOL FEM-2100 instrument at 100 kV; for sample preparation the washed particles were redispersed in a solution of 0.6 M oleic acid in chloroform and dropped on a Formvar-coated copper grid (Plano). Small-angle X-ray scattering (SAXS) measurements of the untreated reaction mixture were carried out on a Nanostar instrument (Bruker AXS GmbH) using $\text{Cu K}\alpha$ radiation and a position sensitive area detector (HiStar). The obtained 2D patterns were azimuthally averaged and corrected for transmission and instrument background.

Results and discussion

From the reaction of titanium isopropoxide in benzyl alcohol we obtained highly crystalline TiO_2 nanoparticles, with the PXRD patterns clearly assignable to the anatase modification, as shown in Fig. 1(a). The experimental data are in good agreement with the reference data for anatase (ICSD database, no. 98-000-9852).

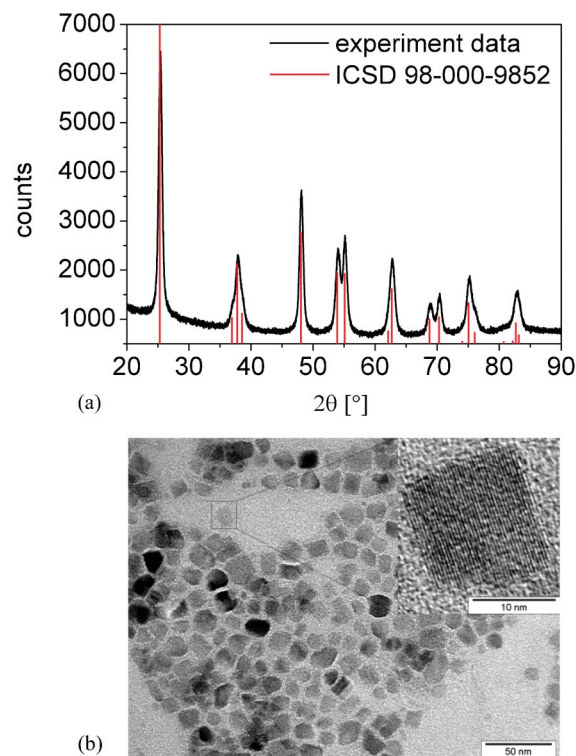


Fig. 1 (a) PXRD pattern of the obtained TiO_2 nanoparticles compared to the anatase reference (ICSD database, no. 98-000-9852), (b) representative TEM images of obtained anatase nanoparticles with a magnification of 180 000 and 1 000 000 (inset; crystallite size ~ 15 nm).

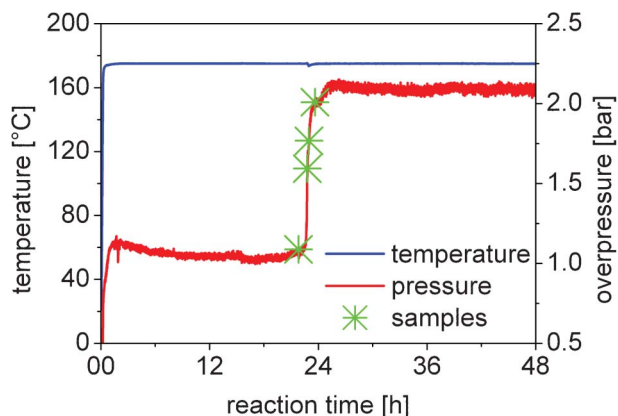


Fig. 2 Development of temperature and pressure within the reactor during the particle synthesis; the green crosses indicate points in time where samples were withdrawn for further analysis.

The sample consists of small crystallites, as recognizable by the peak broadening; applying the Scherrer equation, a crystallite size of 14.5 nm in the [011] direction was calculated with an accuracy of 0.5 nm. From TEM images of typical samples (Fig. 1(b)) we infer that particle sizes and crystallite sizes are equal, meaning that the primary particles are single crystals. Interestingly, in contrast to the synthesis from TiCl_4 , the nanoparticles exhibit a cubic shape and are significantly larger.^{12,13}

By monitoring the reaction process, we observed a sudden and pronounced increase in pressure after a certain reaction time. Fig. 2 shows the development of reaction temperature and pressure within the reactor over time. Upon heating, which was completed within 20 min, a first rise in pressure to 1 bar overpressure was observed, most likely caused by the evaporation of isopropyl alcohol from the reaction mixture due to the ligand exchange reaction. Afterwards, the reaction temperature was kept constant at 175 °C and the pressure remained at this level for about 24 h before suddenly increasing to *ca.* 2 bar overpressure.

To the best of our knowledge, such an instantaneous step-type intrinsic effect has not been described for the nonaqueous synthesis of metal oxide nanoparticles before. For example, in the synthesis of TiO_2 nanoparticles from titanium tetrachloride, which we performed in an open system, only continuous processes were observed,²⁶ and also during the microwave synthesis of ZnO nanoparticles in closed vessels, no pronounced increase in pressure was noted.²⁹ The step-type effect rather resembles the kinetics of the thermal decomposition synthesis.²⁰

Hence, we decided to study the reaction kinetics in detail. First we analyzed the final reaction mixture by ^1H NMR spectroscopy, as illustrated in Fig. 3(a), to determine the organic components formed during the reaction. As elucidated above, the formation of various ethers as organic side products was expected,^{31,33} which could be confirmed by our measurements, detecting predominantly dibenzyl ether but also small amounts of benzyl isopropyl ether and traces of diisopropyl ether. The ^1H NMR spectrum shows, next to the chemical shift of the CH_2 group of benzyl alcohol (2) at 4.57 ppm, clearly a signal of the CH_2 group of dibenzyl ether (3) at a chemical shift of 4.47 ppm,

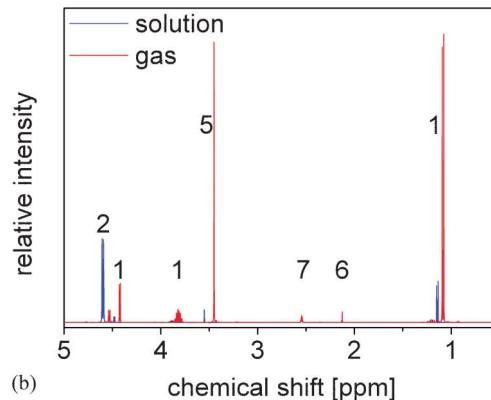
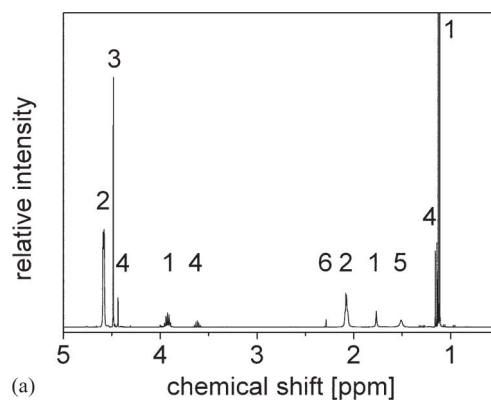
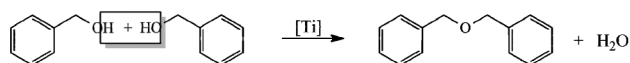


Fig. 3 ^1H NMR spectra of (a) the reaction mixture in CDCl_3 and (b) the reaction mixture (blue) and a sample from the gaseous headspace phase (red) in $\text{DMSO}-d_6$; the peaks are assigned to the components as follows: 1 isopropyl alcohol, 2 benzyl alcohol, 3 dibenzyl ether, 4 benzyl isopropyl ether, 5 water, 6 toluene, 7 DMSO.

and close to it at 4.42 ppm another peak which is assigned to the mixed ether (4). The signals at 3.91 and 3.60 ppm are attributed to the CH groups and at 1.10 and 1.13 ppm to the CH_3 groups of isopropyl alcohol (1) and the mixed ether, respectively. Additionally, a small amount of toluene (6) was detected, stemming from decomposition of benzyl alcohol through heating.³⁴ The molar ratio of benzyl alcohol : dibenzyl ether : benzyl isopropyl ether is calculated from the integrals of the CH_2 groups to about 20 : 4 : 1, whereby the integral of the mixed ether was normalized to 1. Remarkably, the amount of dibenzyl ether is considerably higher than expected from a stoichiometric reaction according to Scheme 1. Therefore we infer that additionally ether is formed *via* a catalytic ether condensation reaction at the titanium centers. The formation of the organic side products was also confirmed by GC/MS measurements (see ESI[†]). Notably, an additional peak is visible in the ^1H NMR spectrum at a chemical shift of 1.49 ppm, which is assigned to water (5). This is somewhat surprising, as the nonaqueous synthesis usually does not result in the formation of significant amounts of free water in the reaction system; only in special cases such as for metal niobates, the formation of excess amounts of water has been reported.³⁵ The presence of water is more visible when using $\text{DMSO}-d_6$ as solvent for the NMR measurement, as shown in Fig. 3(b). Here, the peak at 3.53 ppm

(blue line) can be clearly assigned to water in the reaction mixture. To gain insight into the pressure increase observed during the reaction, we further analyzed samples from the gaseous phase above the reaction mixture by withdrawing gaseous samples through an outlet valve while the mixture was held at the reaction temperature. After cooling to room temperature, a clear liquid was obtained and analyzed by ^1H NMR spectroscopy (Fig. 3(b), red line). In this spectrum, a large quantity of water at 3.42 ppm in a molar ratio of 2 : 1 to isopropyl alcohol (CH_3 : 1.05 ppm, CH : 3.79 ppm, OH : 4.40 ppm) is visible; the slight differences in chemical shift to the solution sample are attributed to the great differences in concentration. Benzyl alcohol is existent only in small amounts (0.28 mol/mol (isopropyl alcohol)); CH_2 : 4.51 ppm. The existence of water in the reaction mixture was also confirmed by Karl Fischer titration (see below for quantification). These findings explain the detection of ethers in the final reaction mixture in much higher amounts than expected for the stoichiometric reaction of the alkoxide. Evidently, *via* a catalytic ether formation at the titanium centers, water is formed through a condensation reaction of the benzyl alcohol solvent (Scheme 2). Hence, the pressure increase can be clearly correlated to the formation of water, which is of high importance for the molecular reaction mechanism. The high reactivity of titanium isopropoxide as well as other metal alkoxides towards water is well known and utilized in aqueous sol-gel synthesis,³⁶ but also in nonaqueous sol-gel methods there are studies about the influence of limited amounts of water on the particle formation.^{37,38} The hydrolysis accelerates the reaction, but in contrast to previously described reaction types water is not added nor formed constantly by organic condensation reactions but is formed in a spontaneous and fast process during the reaction.

The pressure increase also plays an important role in the particle formation, as prior to this step, the reaction mixture appears completely transparent but is turbid afterwards. Therefore, we investigated the processes occurring during the time span of the pressure increase in detail both with regard to the molecular reaction kinetics as well as the particle formation and growth. The formation kinetics of dibenzyl ether, being representative for the sum of ethers, and for water in the reaction mixture during the pressure increase is presented in Fig. 4(a). For better visibility, the time scale is set to 0 at the beginning of the pressure increase. The molar ratio of dibenzyl ether to the total amount of aromatic compounds was calculated by comparing the integrals of the CH_2 group of dibenzyl ether with the aromatic signals from the ^1H NMR spectra of the individual samples. The relative molar amount of the ether after completion of the reaction was determined as nearly 10%, whilst at the beginning of the pressure rise it is rather low with just 1.7%. The subsequent increase for the ether is very similar to the development of pressure and follows first order kinetics, as shown in Fig. 4(b). The data for the kinetics, obtained by fitting



Scheme 2 Condensation of benzyl alcohol to dibenzyl ether at the titanium centers.

the concentration development by an exponential function, is given in Table 1. The molar ratio of water was determined by combining the amount of water determined in the liquid and gaseous phases. The water content in the liquid phase was thereby obtained by Karl Fischer titration; in the gaseous phase it was calculated using the equation of state for real gases estimating the compressibility factor as 0.993.³⁹ The total values were then related to the total amount of aromatic compounds, equivalent to the initial amount of benzyl alcohol. Similar first-order kinetics as in the case of the ether is apparent. We have reported first-order kinetics also before for the formation of side products during the reaction of TiCl_4 in benzyl alcohol,²⁶ but in contrast to our earlier study, the actual molecular mechanisms leading to particle formation do not start after the reaction mixture has reached the target temperature, but at a much later stage at the beginning of the pressure increase and occur within a very limited timescale as compared to the total reaction time.

Fig. 4(c) presents the PXRD patterns of samples taken during and after the pressure rise. An increase of intensity as well as a substantial sharpening of the reflections can be observed. The diminution of the full width at half maximum (FWHM) of reflections with time corresponds to a growth of the particles. As mentioned above, the particle size could be calculated from the PXRD data using the Scherrer equation for the (011) reflection. The particles isolated 10 minutes after the beginning of the pressure increase showed a size of 6.9 nm and are of high crystallinity. During the next 2 hours, the particle size increased to 13.6 nm and within the following 20 hours it increased only slightly further to 14.5 nm. The kinetics of particle growth is illustrated in Fig. 4(d), appearing similar to the formation kinetics of the byproducts and again following first-order kinetics (Table 1). For comparison, the development of pressure is given as well. Initially the particle growth proceeds analogously to the pressure rise, but while the pressure converges to a limiting level, the crystallite growth exhibits a small further increase. The LSW analysis of the development of particle size over time²⁹ (see ESI†) reveals that particle growth occurs *via* two distinct mechanisms, and only the later growth stage might be attributable to Ostwald ripening (according to the modified LSW theory⁴⁰). Our investigations also indicate that with the increase of pressure, corresponding to the formation of water, the formation of the nanoparticles is initiated as well. No particles could be isolated or observed before this step. Moreover, after cessation of the pressure increase, the molecular reactions also do not proceed further, with the amount of ethers remaining constant. Hence, the formation and growth of particles happen concurrently to the formation of the byproducts, most notably water, within the well detectable increase of pressure. With the beginning of the water formation, hydrolysis is initiated and the nanoparticles are formed.

On the other hand, it cannot be excluded in principle that highly stabilized nanoparticles are present before the pressure rise, even though the addition of methanol did not lead to any precipitation. In order to elucidate this issue, SAXS measurements of samples of the reaction mixture withdrawn from the system at different stages of reaction were performed. In Fig. 5 the scattering curves measured for the pure solvent benzyl alcohol, a freshly prepared mixture of the reactants TIP and BnOH as well as the reaction mixture at different stages of the

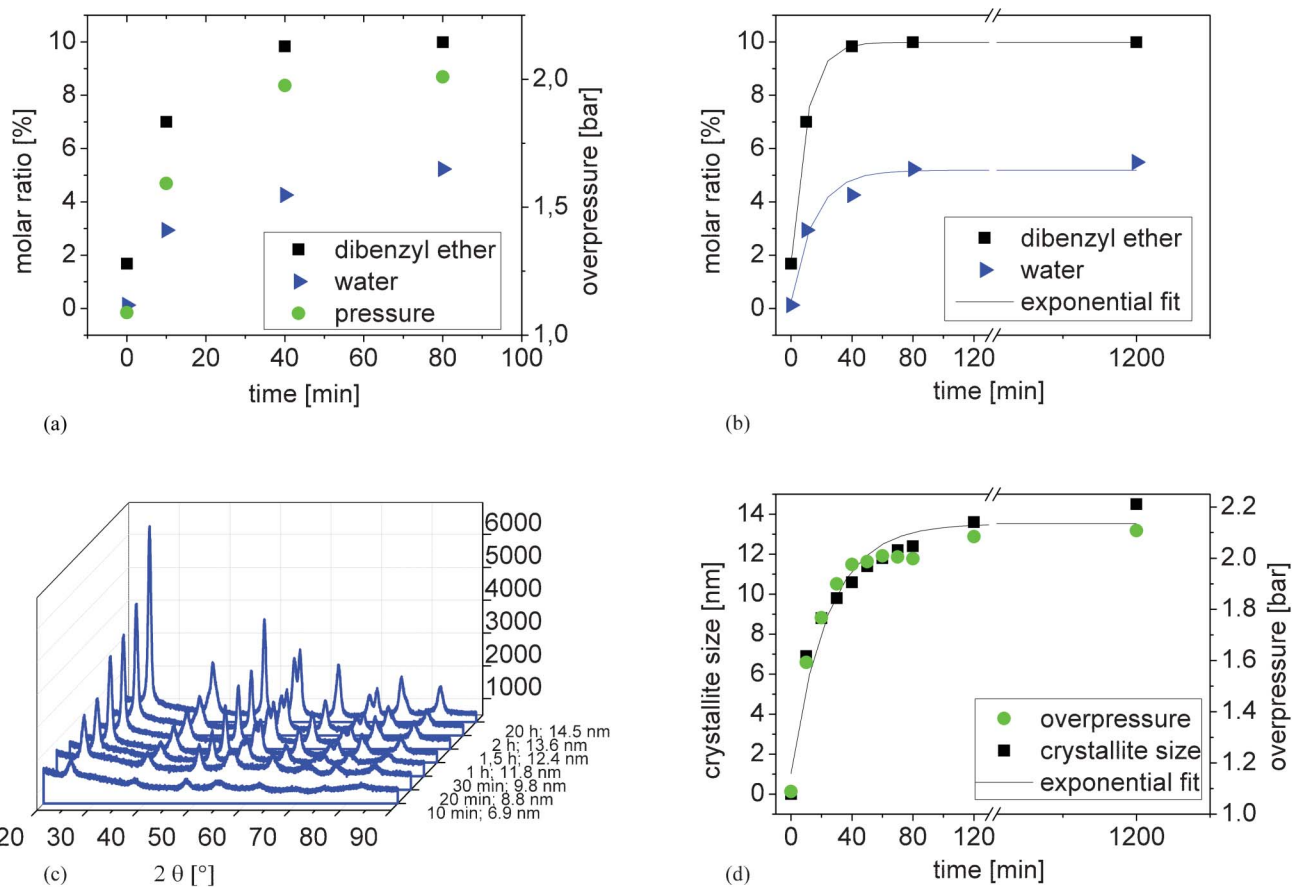


Fig. 4 (a) Concentration development over reaction time for dibenzyl ether and water in comparison to the increase of pressure, (b) first-order kinetics for the formation of dibenzyl ether and water, (c) PXRD data showing the particle growth and the development of crystallinity during reaction time and (d) crystallite size over time, showing the formation kinetics of anatase nanoparticles related to the pressure rise. The little decrease in pressure is caused by sampling. Note: the reaction time is set to 0 at the beginning of the pressure increase.

Table 1 Kinetic data of dibenzyl ether, water and particle formation processes, with c_e = final concentration and d_e = final size (reaction time in h)

	Kinetics	c_e [mol L ⁻¹] or d_e [nm]	A	k [h ⁻¹]
Dibenzyl ether	$c = c_e [1 - A \exp(-kt)]$	9.98	0.83	0.10
Water	$c = c_e [1 - A \exp(-kt)]$	5.18	0.95	0.06
Particle size	$d = d_e [1 - A \exp(-kt)]$	13.52	0.92	0.04

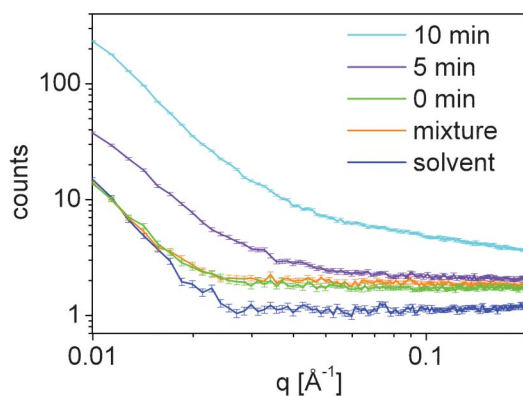


Fig. 5 SAXS measurements of benzyl alcohol, the mixed reactants and the reaction mixture before (0 min), at the beginning of (5 min) and during (10 min) the pressure increase.

pressure rise are displayed. Due to the addition of Ti scattering centers, the curve for the mixture of reactants shows higher intensity at larger q values because of higher contrast as compared to the pure solvent. For low scattering vectors, corresponding to the contribution of bigger structures, the curve however shows the same intensity as the solvent, proving the absence of larger clusters or nanoparticles in the sample. The scattering curve of the sample immediately before the pressure increase shows no significant differences to the precursor solution, verifying that no particles are formed up to this stage of the reaction. With the beginning of the pressure rise, the scattering intensity is strongly enhanced at low q values, evidencing the formation of larger structures. During the pressure rise, the scattering intensity continuously increases, corresponding to particle formation and growth. The increase occurs within a substantially shorter time than reported earlier

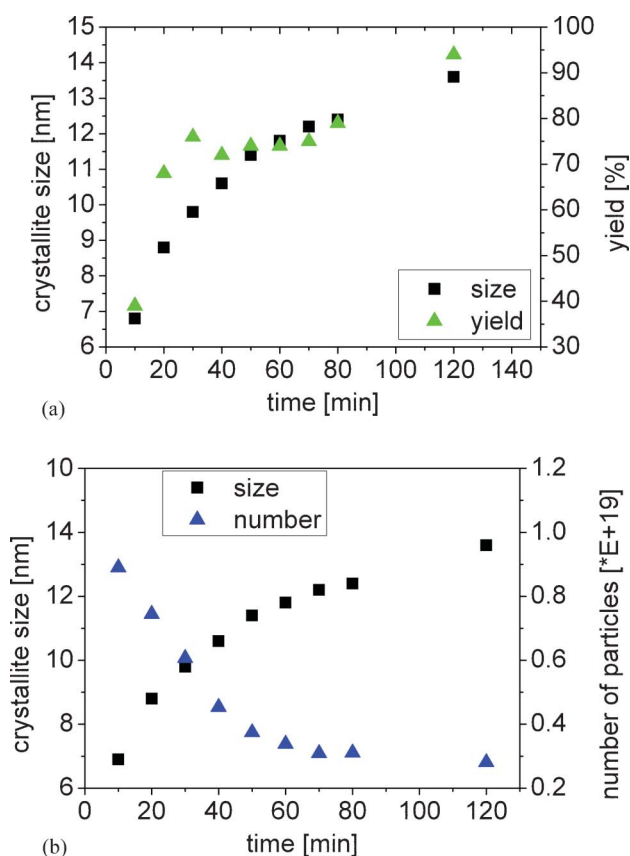


Fig. 6 Development of (a) yield and (b) number of TiO₂ particles over reaction time as determined by TGA. Note: the reaction time is set to 0 at the beginning of the pressure increase.

for the formation of nanoparticles by alkyl halide elimination.⁴¹ A calculation of the size distribution of the scattering structures was not possible with the given measurement setup as the sizes exceeded the resolution of the instrument due to the fast agglomeration of the particles.

To complement the kinetic studies of particle growth, the development of the yield of TiO₂ nanoparticles was determined by TGA measurements. The dried precipitates were heated to 600 °C, leading to decomposition of all organics bound to the particle surface so the actual amount of titanium dioxide was determined. Fig. 6(a) shows the development of the calculated yield over time in comparison to the kinetics of particle size growth. The lower yields at some points are caused by losses during the washing process, so that we assume that the solid content in the reaction mixture increases continuously to almost 100% at the end of the experiment, with analogous kinetics as compared to the particle size and the formation of byproducts. Supposing that the particles possess uniform size, the number of particles at each stage of the reaction can be calculated from the yield as illustrated in Fig. 6(b). The density of TiO₂ is assumed equal to the bulk material as 3.9 g cm⁻³. The slight decrease in the number of particles indicates that only particle growth and possibly some Ostwald ripening happen during the pressure surge but no further nucleation. Hence, the nucleation process is confirmed to occur within a very limited timespan.

Conclusions

We have studied the formation and growth mechanism of TiO₂ nanoparticles for the nonaqueous synthesis by reaction of titanium(IV) isopropoxide in benzyl alcohol. In contrast to the reaction of TiCl₄ *via* alkyl halide elimination, cubic shaped anatase nanoparticles are obtained only after an induction period of almost 24 h. Subsequently, a sudden and pronounced pressure increase was found to occur, being attributable to the formation of water. Concurrently to the pressure increase, fast nucleation and growth of the nanoparticles were observed, presumably being caused by a hydrolysis of the precursor species. At the same time the rate of formation of organic ethers increases rapidly, with the formed quantities clearly exceeding the stoichiometric amount expected from the nonaqueous reaction mechanism. Hence, the spontaneous water formation is explained by a catalytic ether condensation of benzyl alcohol at the titanium centers. Although the formation of excess amounts of water has been identified before for the synthesis of metal niobates, it has not been reported for the simple reaction of a metal alkoxide in benzyl alcohol nor for titanium as the metal species. Moreover, the particle formation and growth are initiated at the beginning of the pressure increase and show analogous kinetics as the water formation and ether formation reactions, except for subsequent Ostwald ripening processes. SAXS measurements proved the absence of any nanoparticles before the pressure surge, evidencing the crucial influence of the water formation on the particle formation kinetics. Therefore, the observed mechanism determines the formation and also the properties of the formed nanoparticles and possibly is the reason for the strong differences in morphology as compared to the TiCl₄-benzyl alcohol system. Because the reaction of a metal alkoxide in an alcohol is a widely employed approach for the synthesis of metal oxide nanostructures, the mechanisms reported here might occur in a variety of other systems, also especially for the metal niobates. Moreover, the nonaqueous synthesis is known to lead to nanoparticles with very different sizes and morphologies for different systems, which yet can only partially be explained. As the formation of well-faceted nanocrystals is shown here to be greatly facilitated by catalytic water formation, the occurrence of this mechanism, possibly only to a small extent in other systems, might be a general explanation for the highly different product particle morphologies.

Acknowledgements

This work was financially supported by the Deutsche Forschungsgemeinschaft (DFG), grant GA 1492/3-1. The authors would like to thank Mr. Bilal Temel from the Institute for Particle Technology, TU Braunschweig, for the XRD measurements, Dr. Till Beuerle, Institute of Organic Chemistry, TU Braunschweig, for the GC/MS measurements and Mrs. Ingrid Zenke from the Department of Biomaterials, Max Planck Institute of Colloids and Interfaces, Potsdam, for the SAXS measurements. Dr. Kerstin Ibrom, Institute of Organic Chemistry, TU Braunschweig, is acknowledged for helpful discussions on the NMR analyses.

References

- 1 A. Mills, R. H. Davies and D. Worsley, *Chem. Soc. Rev.*, 1993, **22**, 417–425.
- 2 A. L. Linsebigler, G. Lu and J. T. Yates, *Chem. Rev.*, 1995, **95**, 735–758.
- 3 J. Peral, X. Domenech and D. F. Ollis, *J. Chem. Technol. Biotechnol.*, 1997, **70**, 117–140.
- 4 E. Stathatos, D. Tsiourvas and P. Lianos, *Colloids Surf., A*, 1999, **149**, 49–56.
- 5 Y. Kikuchi, K. Sunada, T. Iyoda, K. Hashimoto and A. Fujishima, *J. Photochem. Photobiol., A*, 1997, **106**, 51–56.
- 6 B. O'Regan and M. Grätzel, *Nature*, 1991, **353**, 737–740.
- 7 M. Grätzel, *Acc. Chem. Res.*, 2009, **42**, 1788–1798.
- 8 I. Mora-Seró and J. Bisquert, *J. Phys. Chem. Lett.*, 2010, **1**, 3046–3052.
- 9 T. Miyasaka, *J. Phys. Chem. Lett.*, 2011, **2**, 262–269.
- 10 D. M. Blake, P. C. Maness, Z. Huang, E. J. Wolfrum, J. Huang and W. A. Jacoby, *Sep. Purif. Methods*, 1999, **28**, 1–50.
- 11 S. Ivankovic, M. Gotic, M. Jurin and S. Music, *J. Sol-Gel Sci. Technol.*, 2003, **27**, 225–233.
- 12 A. S. Gurav, Z. Duan, L. Wang, M. J. Hampden-Smith and T. T. Kodas, *Chem. Mater.*, 1993, **5**, 214–216.
- 13 F. E. Kruijs, H. Fissan and A. Peled, *J. Aerosol Sci.*, 1998, **29**, 511–535.
- 14 B. L. Cushing, V. L. Kolesnichenko and C. J. O'Connor, *Chem. Rev.*, 2004, **104**, 3893–3946.
- 15 M. Niederberger, M. H. Bartl and G. D. Stucky, *J. Am. Chem. Soc.*, 2002, **124**, 13642–13643.
- 16 M. Niederberger, M. H. Bartl and G. D. Stucky, *Chem. Mater.*, 2002, **14**, 4364–4370.
- 17 G. Garnweitner and M. Niederberger, *J. Am. Ceram. Soc.*, 2006, **89**, 1801–1808.
- 18 N. Pinna and M. Niederberger, *Angew. Chem., Int. Ed.*, 2008, **47**, 5292–5304.
- 19 M. Niederberger and G. Garnweitner, *Chem.–Eur. J.*, 2006, **12**, 7282–7302.
- 20 S. G. Kwon, Y. Piao, J. Park, S. Angappane, Y. Jo, N.-M. Hwang, J.-G. Park and T. Hyeon, *J. Am. Chem. Soc.*, 2007, **129**, 12571–12584.
- 21 S. G. Kwon and T. Hyeon, *Acc. Chem. Res.*, 2008, **41**, 1696–1709.
- 22 V. K. LaMer and P. H. Dinegar, *J. Am. Chem. Soc.*, 1950, **70**, 4847–4854.
- 23 V. K. LaMer, *Ind. Eng. Chem.*, 1952, **44**, 1270–1277.
- 24 C. B. Murray, D. J. Norris and M. G. Bawendi, *J. Am. Chem. Soc.*, 1993, **115**, 8706–8715.
- 25 J. Y. Rempel, M. G. Bawendi and L. F. Jensen, *J. Am. Chem. Soc.*, 2009, **131**, 4479–4489.
- 26 G. Garnweitner and C. Grote, *Phys. Chem. Chem. Phys.*, 2009, **11**, 3767–3774.
- 27 B. Ludi, M. J. Süess, I. A. Werner and M. Niederberger, *Nanoscale*, 2012, **4**, 1982–1995.
- 28 I. Bilecka and M. Niederberger, *Electrochim. Acta*, 2010, **55**, 7717–7725.
- 29 I. Bilecka, P. Elser and M. Niederberger, *ACS Nano*, 2009, **3**, 467–477.
- 30 I.-M. Grabs, C. Bradtmöller, D. Menzel and G. Garnweitner, *Cryst. Growth Des.*, 2012, **12**, 1469–1475.
- 31 N. Pinna, G. Garnweitner, M. Antonietti and M. Niederberger, *Adv. Mater.*, 2004, **16**, 2196–2200.
- 32 G. Garnweitner and M. Niederberger, *J. Mater. Chem.*, 2008, **18**, 1171–1182.
- 33 M. Niederberger, G. Garnweitner, N. Pinna and M. Antonietti, *J. Am. Chem. Soc.*, 2004, **126**, 9120–9126.
- 34 A. R. Katritzky and M. Balasubramanian, *Energy Fuels*, 1990, **4**, 499–505.
- 35 L. Zhang, G. Garnweitner, I. Djerdj, M. Antonietti and M. Niederberger, *Chem.–Asian J.*, 2008, **3**, 746–752.
- 36 J. Livage, M. Henry and C. Sanchez, *Prog. Solid State Chem.*, 1988, **18**, 259–341.
- 37 M. Inoue, H. Kominami and T. Inui, *Appl. Catal., A*, 1995, **121**, L1–L6.
- 38 H. Kominami, Y. Takada, H. Yamagiwa and Y. Kera, *J. Mater. Sci. Lett.*, 1996, **15**, 197–200.
- 39 R. H. Perry and D. Green, *Perry's Chemical Engineers' Handbook*, McGraw-Hill, New York, 1984.
- 40 I. M. Lifshitz and V. V. Slyozov, *J. Phys. Chem. Solids*, 1961, **19**, 35–50.
- 41 G. V. Jensen, M. Bremholm, N. Lock, G. R. Deen, T. R. Jensen, B. B. Iversen, M. Niederberger, J. S. Pedersen and H. Birkedal, *Chem. Mater.*, 2010, **22**, 6044–6055.